Glycerol kinase from *Escherichia coli* and an Ala65→Thr mutant: the crystal structures reveal conformational changes with implications for allosteric regulation

Michael D Feese[1], H Rick Faber[2], Cory E Bystrom[2], Donald W Pettigrew[3] and S James Remington[2]*

Background: Glycerol kinase (GK) from *Escherichia coli* is a velocity-modulated (V system) enzyme that has three allosteric effectors with independent mechanisms: fructose-1,6-bisphosphate (FBP); the phosphocarrier protein IIA^{Glc}; and adenosine nucleotides. The enzyme exists in solution as functional dimers that associate reversibly to form tetramers. GK is a member of a superfamily of ATPases that share a common ATPase domain and are thought to undergo a large conformational change as an intrinsic step in their catalytic cycle. Members of this family include actin, hexokinase and the heat shock protein hsc70.

Results: We report here the crystal structures of GK and a mutant of GK (Ala65→Thr) in complex with glycerol and ADP. Crystals of both enzymes contain the same 222 symmetric tetramer. The functional dimer is identical to that described previously for the IIA^{Glc}–GK complex structure. The tetramer interface is significantly different, however, with a relative 22.3° rotation and 6.34 Å translation of one functional dimer. The overall monomer structure is unchanged except for two regions: the IIA^{Glc}-binding site undergoes a structural rearrangement and residues 230–236 become ordered and bind orthophosphate at the tetramer interface. We also report the structure of a second mutant of GK (Ile474→Asp) in complex with IIA^{Glc}; this complex crystallized isomorphously to the wild type IIA^{Glc}–GK complex. Site-directed mutants of GK with substitutions at the IIA^{Glc}-binding site show significantly altered kinetic and regulatory properties, suggesting that the conformation of the binding site is linked to the regulation of activity.

Conclusions: We conclude that the new tetramer structure presented here is an inactive form of the physiologically relevant tetramer. The structure and location of the orthophosphate-binding site is consistent with it being part of the FBP-binding site. Mutational analysis and the structure of the IIA^{Glc}–GK(Ile474→Asp) complex suggest the conformational transition of the IIA^{Glc}-binding site to be an essential aspect of IIA^{Glc} regulation.

Addresses: [1]Central Laboratories for Key Technology, 1-13-5 Fukuura, Kanazawa, Yokohama 236, Japan, [2]Institute of Molecular Biology and Departments of Physics and Chemistry, University of Oregon, Eugene, Oregon 97403, USA and [3]Department of Biochemistry and Biophysics, Texas A&M University, College Station, Texas 77483, USA.

*Corresponding author.
E-mail: jim@uoxray.uoregon.edu

Key words: allostery, cooperativity, crystal structure, glycerol kinase

Received: **19 June 1998**
Revisions requested: **20 July 1998**
Revisions received: **27 July 1998**
Accepted: **13 August 1998**

Structure 15 November 1998, **6**:1407–1418
http://biomednet.com/elecref/0969212600601407

Introduction

Glycerol kinase from *Escherichia coli* (GK, EC 2.7.1.30; ATP glycerol 3-phosphotransferase) was first isolated and studied by Lin and colleagues in the 1960s. They showed that the enzyme catalyzes the MgATP-dependent phosphorylation of glycerol to produce *sn*-glycerol-3-phosphate (G3P), and is the rate-limiting enzyme in the utilization of glycerol [1,2]. The enzyme was also shown to be subject to feedback regulation by the glycolytic intermediate fructose-1,6-bisphosphate (FBP) [3]. Thorner and Paulus [4,5] demonstrated that GK was a tetramer of identical subunits and was allosterically regulated by FBP in a purely non-competitive (velocity modulated or V system) [5] manner with respect to both substrates. In a tour de force of kinetic and hydrodynamic studies [6–8], de Riel and Paulus revealed that the enzyme actually exists in a dimer↔tetramer equilibrium at physiological concentrations ($K_D \sim 5 \times 10^{-8}$) and that FBP binds to and stabilizes only the tetrameric form, decreasing the dimer–dimer dissociation constant by up to four orders of magnitude.

More recently, the phosphoenolpyruvate: glycose phosphotransferase system (PTS) phosphocarrier protein IIA^{Glc} (M_r 18 000, also referred to as III^{Glc} in older literature) has been identified as a second allosteric effector of GK [9,10]. Mutational analysis showed IIA^{Glc} regulation to be distinct from that of FBP, and its effect is independent of GK concentration over a wide range [10].

Finally, GK displays homotropic allosteric regulation with respect to nucleotide concentration [5], and shows 'half-of-the-sites binding' for ATP, ADP and glycerol (i.e. a functional dimer has one high-affinity and one low-affinity active site for substrates) [11]. Half-of-the-sites binding suggests an intrinsic asymmetry in the subunit structure that is often related to allosteric regulation. It has been reported that GK is stimulated by interaction with the membrane-bound glycerol facilitator [12], suggesting yet another level of allosteric regulation.

GK is a member of a superfamily of ATPases [13,14] that, although dissimilar in amino acid sequence and function, have similar tertiary folds [15–17] and probably share the same catalytic mechanism. These enzymes — GK [5], hexokinase [18–21], actin [22,23] and the heat shock cognate protein hsc70 [24] — are thought to undergo large conformational changes as an intrinsic step in their reaction cycle.

The wild-type gene for *E. coli* GK has been cloned and the sequence determined [25]; the gene encodes for a protein of 501 amino acids (M_r 56,099). The crystal structure of the regulatory complex of GK and IIA^{Glc} with bound ADP and glycerol [26] has been solved. This structure shows GK to be a tetramer (tetramer I) with crystallographically enforced *222* point symmetry. IIA^{Glc} is bound to a short, solvent-exposed 3_{10} helix ~30 Å from the active site. The IIA^{Glc}–GK interface has also been shown to form an intermolecular Zn(II)-binding site that significantly enhances IIA^{Glc} inhibition *in vitro* [27,28]). Amino acid substitutions that affect allosteric regulation of GK by FBP or IIA^{Glc}, or alter the subunit dissociation properties of the enzyme, have been studied [10,13,29–31].

In this paper, we present the crystal structures of wild-type GK and a mutant, Ala65→Thr (A65T). The A65T mutation was identified by random mutagenesis and screening for loss of function in glucose control of glycerol metabolism. The mutation eliminates FBP regulation and tetramerization of GK *in vitro* while having little effect on IIA^{Glc} regulation or the catalytic constants of the enzyme [31]. Although they were crystallized in different unit cells, both wild-type and A65T GK exist in the same tetrameric form (tetramer II) in the crystal. Tetramer II has nearly exact *222* point symmetry, but has altogether different dimer–dimer interactions than tetramer I. The IIA^{Glc}-binding helix, residues 472–481, changes conformation in tetramer II. In addition, the loop region from residues 230–236, which is disordered in tetramer I, becomes ordered as part of the tetramer II interface and forms a binding site for orthophosphate and sulfate ions in the wild-type and A65T GK structures, respectively. The implications of these results for tetramer formation and regulation are discussed in view of the altered kinetic behavior of A65T GK and several other amino acid substitutions.

Results

Crystal packing

Both the wild-type and A65T forms of GK crystallize in space group $P2_1$ with a tetramer of *222* point symmetry as the asymmetric unit. The monomers of each tetramer are designated O, X, Y and Z. The tetramer has the same subunit–subunit interactions in both crystal forms, designated the O–X and O–Y interfaces. Both crystal forms have the same crystal-packing interactions in the *a* and *b* unit-cell directions. The contacts in the *c* direction are somewhat different, however, and lead to a 10.3° increase in the β angle in the A65T crystal form. In the A65T unit cell, the tetramers of adjoining unit cells in the *c* direction are shifted by ~19.6 Å relative to the wild type unit cells, along an axis parallel to the *a* unit-cell edge. The result is a unit cell with nearly the same cell edge lengths but different β angles. The unit-cell volume in crystals of A65T GK is essentially identical to that of wild type. Statistics of the refined models are presented in Table 1.

Mainchain conformation and domain organization

The structure of GK has now been refined against data from three different crystal forms (Table 1) and the monomer has an essentially identical structure in all crystal forms seen to date. The monomer consists of two major domains (I and II) separated by a rather deep active-site cleft. The domains have been further subdivided according to topologically equivalent structures among the members of the ATPase superfamily to which GK belongs (Figure 1; Figure 3a of reference [26]). Subdomains IA and IIA form the ATPase core — both contain a five-stranded β sheet flanked by three α helices. Among the family members, various insertions and additions to this core structure occur in similar locations, but have completely different tertiary structures [14].

In GK, subdomains IB, IIB and IC are formed from insertions into this common core, whereas subdomain IIC is an extension of the C terminus of the polypeptide chain (see Figure 3a of reference [26]). It is interesting that each of these subdomains has a unique and well-defined role in the enzyme's structure and/or function. The dimer (O–Y) interface is formed by subdomains IIB and IIC, and the tetramer (O–X) interface is formed by subdomains IA and IC. The orthophosphate-binding site is formed by IC, and the IIA^{Glc}-binding site is part of IIC.

Subdomain IB forms part of the glycerol-binding site, whereas subdomain IIB forms the twofold O–Y interface of the functional GK dimer and is presumably involved in monomer–monomer communication that results in half-of-the-sites reactivity. Subdomain IIB is topologically equivalent to the corresponding subdomains of hsc70 and actin, but its tertiary structure is completely different: two β strands from each monomer of the dimer form a four-stranded intersubunit antiparallel β sheet, with the

Table 1

Data collection and refinement statistics.

Data set	Wild type	A65T	IIA^{Glc}–GK (I474D)
Resolution (Å)	20.0–2.62	37.0–2.37	21.1–2.37
Number of observations	190,143	132,331	43,321
Number of reflections	58,942	69,682	26,471
Completeness (%)	84	74	72
Wilson B factor	20.9	32.3	36.5
R_{sym} (%)*	7.6	6.8	5.1
Average B factor of protein model			
all atoms	30.7	38.2	37.9
protein backbone	26.7	34.8	36.6
sidechains	34.8	41.7	39.4
Number of protein atoms	15,639	15,621	4909
Number of heteroatoms	142	54	39
Number of water molecules	200	140	58
Rms deviations of the model†			
bonds (Å)	0.020	0.019	0.019
angles (°)	2.99	2.92	3.05
planarity (Å)	0.019	0.019	0.019
restrained B factors (Å^2)	9.87	9.31	8.58
R_{cryst} (%)‡	14.6	16.6	17.5

*$R_{sym} = \Sigma(I-<I>)/\Sigma<I>$. †Target values are 0.02 Å for bond lengths and planarity, 3.0° for bond angles and 6.0 Å^2 for restrained B factors derived from high-resolution (~1.6 Å) structures. ‡$R_{cryst} = \Sigma||F_{obs}|-|F_{calc}||/\Sigma|F_{obs}|$.

β strand from residues 361–366 hydrogen bonding to its symmetry equivalent across the O–Y interface.

The subdomain IC insertion is at a new location between the first α helix and the first β strand of the IA subdomain and is not found in other members of the ATPase superfamily. This subdomain is a mixed α/β structure containing two strands of parallel β sheet, a β hairpin and two short α helices. The glycine-rich loop (residues 228–236) immediately following one of the β strands forms the orthophosphate- and sulfate-binding site at the twofold O–X interface. In the GK–IIA^{Glc} complex structure residues 230–236 of this loop are completely disordered.

Subdomain IIC consists of a 150-residue C-terminal extension of the IIA core subdomains. This domain forms the IIA^{Glc}-binding site and part of the O–Y interface, and consists of two α helices and a single β strand that wrap around the outside of the IIA subdomain. In the IIA^{Glc}–GK complex, two turns of 3_{10} helix (residues 473–478) form part of the IIA^{Glc}-binding site. As described in detail in a following section, in the present structures this region changes conformation to make a short strand-like region and an extra turn at the beginning of the last α helix of the domain.

It is very interesting that both subdomains IC and IIC, which form effector-binding sites, are integrated into the ATPase core fold by contributing extra β strands to the central β sheets of the IA and IIA subdomains, respectively (Figure 1). This provides a possible structural basis for long-range communication of the effector-binding sites with the active site.

Changes in quaternary structure

The interactions that form the O–X interface between the functional GK dimers in tetramer II are completely different from those observed in tetramer I (Figures 2 and 3). Relative to tetramer I, in tetramer II one functional dimer undergoes a screw rotation of 22.3° with a 6.34 Å translation, bringing the functional dimers of the tetramer closer together. The result is a striking change in the protein–protein interactions between the dimers. In tetramer I, each monomer contacts every other monomer

Figure 1

Stereoview of the GK tetramer II monomer illustrating the domain structure and effector-binding sites. The ATPase core subdomains are shown in grey; subdomains IB, IIB, IC and IIC are shown in red and labeled accordingly. The extra β strands contributed to the ATPase core β sheets by subdomains IC and IIC are shown in yellow. The IIA^{Glc} and orthophosphate (putative FBP) binding regions are labeled accordingly. ADP and glycerol (shown as ball-and-stick structures) are bound between the core β sheets of the ATPase domain.

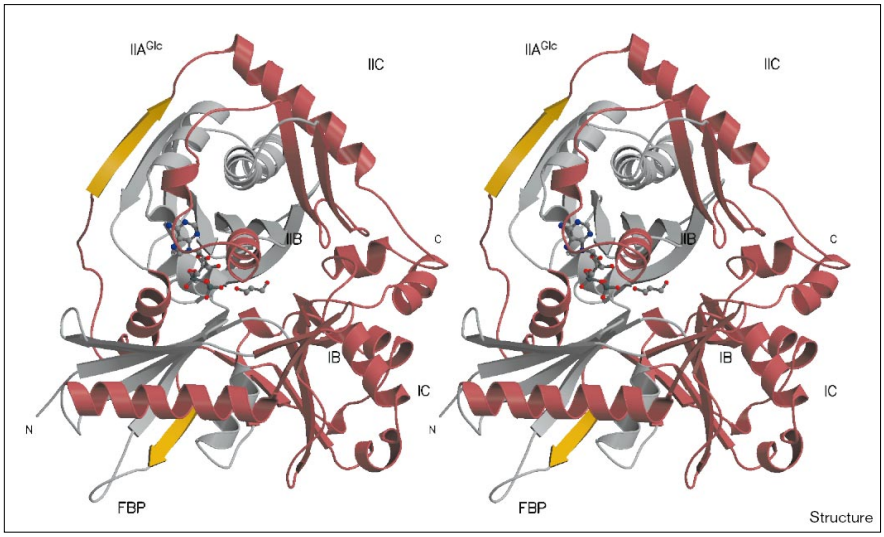

Figure 2

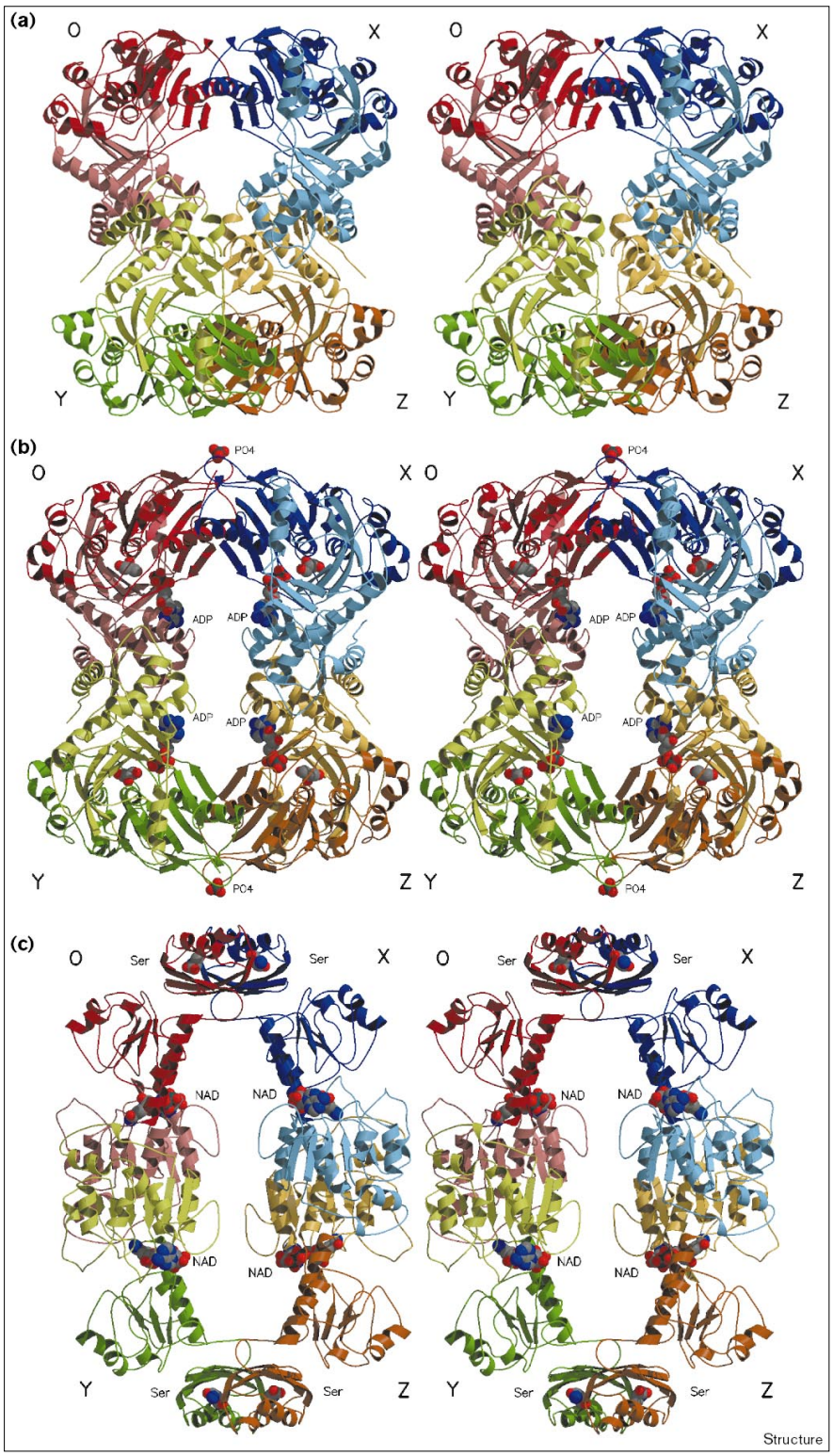

Comparison of GK tetramers I and II and the phosphoglycerate dehydrogenase (PGDH) tetramer. **(a)** GK tetramer I. The O, X, Y and Z monomers are colored red, blue, green and orange, respectively, with domain I of each monomer in a darker shade than domain II. The structure of IIA^{Glc}, which was part of the tetramer I, has been omitted for clarity. **(b)** GK tetramer II with the O and X chains oriented similarly to those of GK tetramer I. The tetramer is colored as in (a) and bound orthophosphate, ADP and glycerol are shown as space-filling models. **(c)** The PGDH tetramer. Monomers are labeled and colored in the same manner as for the GK tetramer, with the substrate-binding and regulatory domains in a darker shade than the NADH-binding domains. Bound NADH and serine molecules are shown as space-filling models. As in GK, the O–Y interface is much more extensive than the O–X interface.

(the O–Y, O–X and O–Z interfaces). In contrast, in tetramer II only the O–Y and O–X interfaces exist. The O–Z interface, which has a mean ΔASA (total change in solvent-accessible surface area divided by the number of

Figure 3

Helical interactions at the tetramer-forming interface (O–X). **(a)** Stereoview of the α-helical interactions at the O–X interface of tetramer II. **(b)** Stereoview of the α-helical interactions at the O–X interface of tetramer I.

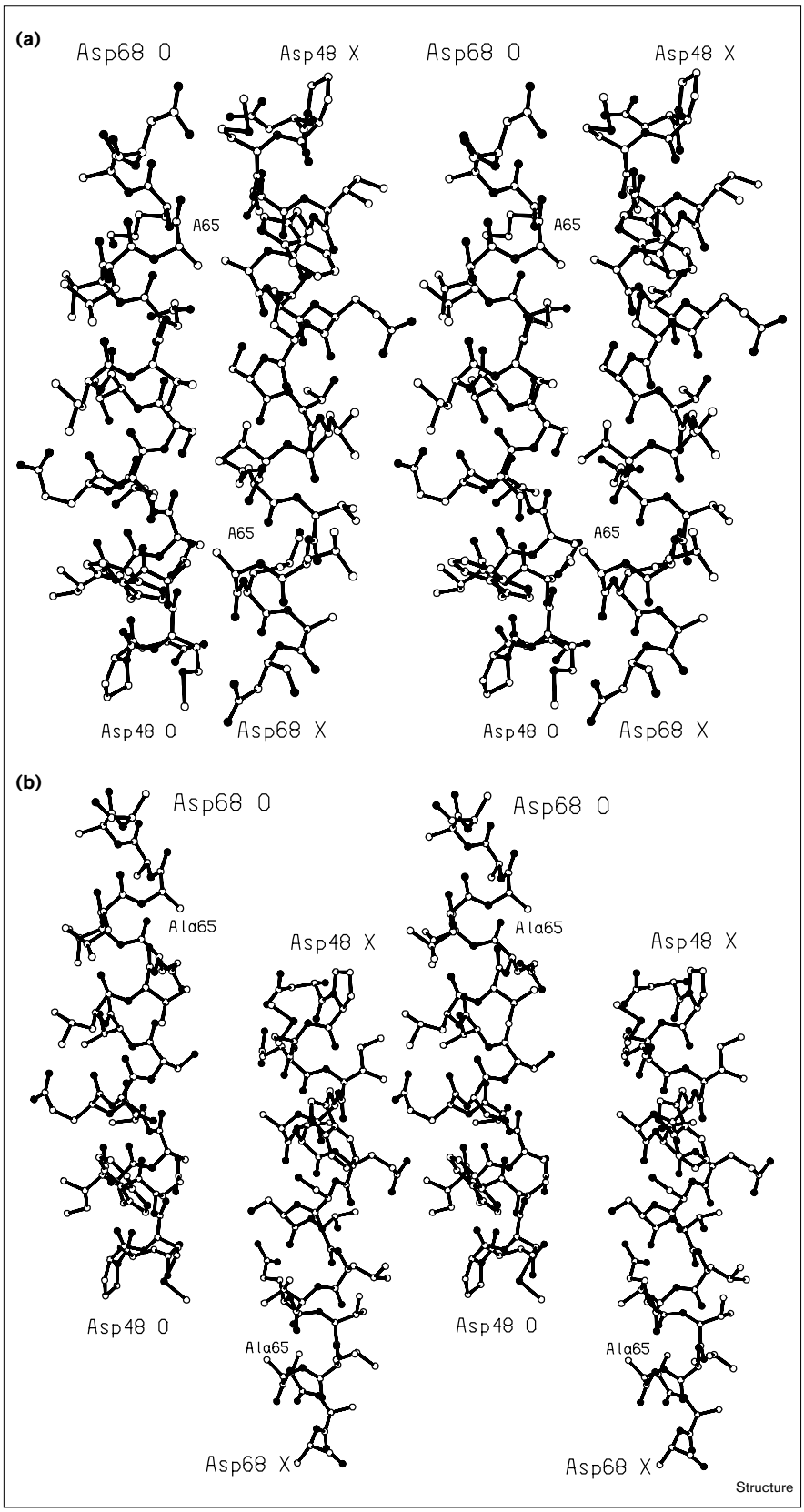

Figure 4

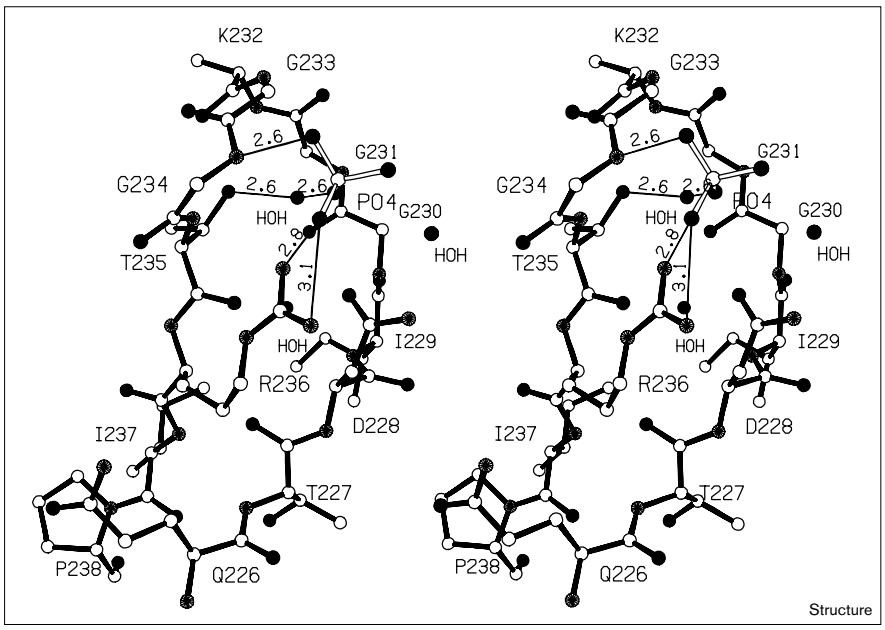

Stereoview of one loop of the orthophosphate-binding site of the GK tetramer II. The bound orthophosphate molecule is shown with open bonds. Apparent hydrogen bonds between the bound orthophosphate and the protein and one bound water molecular are shown as thin lines with labels showing the interatomic distances (in Å).

interacting partners [32]) of 313 Å^2, is completely gone — with ~9 Å between the formerly interacting surfaces. The O–X interface becomes much more extensive in tetramer II (Figure 3a). In tetramer I, the O–X interface comprises only a symmetric antiparallel interaction between the first α helices (residues 49–67) of the IA subdomains (Figure 3b) — this interface has a mean ΔASA of 204 Å^2. In tetramer II, the interface comprises the first α helices of the IA core subdomains and the orthophosphate-binding site. The glycine-rich loops (residues 228–236) fold over the top of the α helices, binding an orthophosphate or sulfate ion between them directly on the tetramer twofold axis (Figure 4). The tetramer II O–X interface has a mean ΔASA of 837 Å^2 (461 Å^2 polar and 376 Å^2 hydrophobic surface area). A comparison of the two tetrameric forms of GK (I and II) are illustrated in Figures 2a and b.

The A65T mutation has been shown in a previous study [31] to completely abolish both FBP regulation and tetramer formation in solution (as observed by gel-permeation chromatography) without notably altering activity or regulatory behavior with respect to IIA^{Glc}. In the crystal, however, the A65T mutant of GK forms a tetramer virtually identical to the wild-type tetramer. The probable reason for this is that the crystal lattice energy or high protein concentration in crystallization experiments drives tetramer formation that does not occur in normal solution conditions. Although Ala65 is part of the α helix (residues 49–67) that forms the largest contact of the tetramer II interface, it has no intermolecular contacts within 3.5 Å. Threonine of the A65T mutant, on the other hand, makes a number of intermolecular interactions. The interface α helices are slightly flexed so that the Cβ atoms of Thr65 and Ala54 move ~1.54 Å apart to accommodate the Cγ2 atom of Thr65 that makes van der Waals contact with Cα and Cβ of Ala54. It seems likely that this steric clash prevents tetramer formation of the A65T mutant in solution. Thr65 Oγ1 hydrogen bonds to Ser57 Oγ and makes van der Waals contact with Trp53 Nε. Despite these extra contacts, the mean ΔASA of the O–X interface in the A65T mutant is ~11 Å^2 less than that of wild type.

The functional dimer O–Y interface remains essentially unchanged among all of the structures examined; there is an average 1.48° rotation and 0.43 Å translation between the monomers of the functional dimers of tetramer II, relative to tetramer I. The mean ΔASA for the O–Y interface is 1776 Å^2 in tetramer I and 1766 Å^2 in tetramer II.

A convenient gauge of the importance of protein–protein interactions in crystal structures is the gap index — the ratio of the solvent inaccessible volume between two interacting surfaces to the total buried solvent-accessible surface area of one of the partners in the interaction [32]. Interfaces with smaller gap indices are more complimentary and have better van der Waals contacts, and thus are more likely to be biologically relevant. The O–Y interface has a very small gap index of 0.89 in accordance with it being a permanent functional interface that forms a continuous β sheet. The gap index for the tetramer I O–X interface is 19.41, reflecting the non-optimal distance and

orientation between the interacting α helices. In contrast, the gap index for the tetramer II O–X interface is 1.8 — within the range expected for a biologically relevant homoprotein interaction [32]. Thus, it seems likely that tetramer II, rather than tetramer I, is the functional tetramer involved in regulation by FBP. Considering that the crystal-packing contacts in the IIA^{Glc}–GK complex [26] are much more extensive than the dimer–dimer contacts of tetramer I, it seems likely that tetramer I is an artifact of crystal packing rather than a biologically relevant form of the enzyme.

GK was the first V-system enzyme to be studied by X-ray crystallography, however, the structure of a second, phosphoglycerate dehydrogenase (PGDH), has recently been described [33]. The monomer structures of GK and PGDH are different in every respect, however, the overall tetrameric configurations of the two enzymes are stunningly similar (Figures 2b and c). Whether there is a connection between V-system regulation and this particular quaternary configuration is at present unclear, but the similarity is worth noting.

Changes in monomer structure

There are two regions of distinct structural change within the GK monomers of tetramer I and tetramer II: the IIA^{Glc}-binding site undergoes a secondary structure change; and the loop comprising residues 230–236, which is disordered in tetramer I, becomes well ordered in tetramer II and forms the orthophosphate- and sulfate-binding site. Otherwise, the individual monomers of tetramer II are quite similar to each other and to those of tetramer I. Excluding the IIA^{Glc}- and orthophosphate-binding sites (residues 230–236 and 472–480, respectively) the average root mean square (rms) deviation for the six possible least squares Cα overlays between pairs of tetramer II monomers is 0.40 Å; for their overlays with the tetramer I monomer the rms deviation is 0.44 Å.

The IIA^{Glc}-binding site

As described previously [26], in tetramer I the IIA^{Glc}-binding site located in the IIC subdomain contains two turns of exposed 3_{10} helix (residues 473–478) that make an ~45° bend with respect to the C-terminal α helix (residues 479–499). In tetramer II this region adopts a completely different secondary structure (Figures 5a and b). The 3_{10} helix relaxes into a strand-like structure, allowing residues 476–478 to become part of the C-terminal α helix, extending it by almost a full turn. The direction of Ile474 is reversed so that it fits into the cleft between the C-terminal α helix and the second α helix of the IIA subdomain, with a total movement of ~4 Å for its Cα atom and ~10 Å for its Cβ atom. The Cα atom of Glu475 also makes a large movement of ~5 Å. Arg479 moves inwards to make hydrogen bonds to the backbone carbonyls of Asp424 and Ile474. This conformational change is essentially restricted within the range of residues 472–479 and is seen in seven of the eight monomers in the two crystal forms. For reasons that are not entirely clear, monomer Z of the wild type appears to have roughly the same conformation as seen in tetramer I, but the density is poor in all cases. The average B factor for all atoms from residues 470–480 is 56.2 $Å^2$ for both wild-type and A65T GK; the overall average B factors are 30.8 $Å^2$ for wild type and 38.2 $Å^2$ for the A65T mutant.

The secondary structure change of the 3_{10} helix at the IIA^{Glc}-binding site is a clear example of induced fit in inhibitor binding. Most observed conformational changes in proteins involve changes in loop structures, relatively rigid movements of existing secondary structure, and hinge-bending motions [34]. Recently, however, a number of secondary structure transitions similar to that observed here, and also involved in regulation, have been identified [35–37]. In addition, members of the serpin family of serine protease inhibitors undergo similar secondary structural changes as an activation mechanism [38], and the prion protein has been shown to undergo global secondary structure changes in the transition from the native to the pathogenic form [39].

In view of this conformational change, site-directed mutagenesis was used to assess the roles of two residues at the GK–IIA^{Glc} interface. The Ile474→Asp (I474D) and Arg479→Asp (R479D) mutant GKs were constructed and characterized. The effects of the substitutions on the initial-velocity parameters are shown in Table 2. Both of the substitutions decrease V_{max} to about 10% of the wild-type value, indicating long-range communication between the secondary structure in this region of the protein and the active site. The substrate Michaelis constants are decreased about six- to eightfold and the apparent affinity for substrates is increased about two- to fourfold as shown by the values for $K_{i,ATP}$.

It is interesting that these perturbations decrease the catalytic activity in a manner that is analogous to that obtained upon IIA^{Glc} binding. The substitutions also alter the regulatory properties of GK, but they have different effects. Regulation by FBP is not affected by the R479D substitution, but the I474D substitution increases the apparent affinity for FBP about fivefold (data not shown). For the R479D mutant, no inhibition by IIA^{Glc} is observed in assays at pH 7.0 at IIA^{Glc} concentrations of up to 25 μM. Thus, the R479D substitution reduces the apparent affinity for IIA^{Glc} by at least 250-fold relative to the wild-type GK. In contrast, the I474D mutant GK is inhibited ~20% at 25 μM IIA^{Glc}, which is consistent with a decrease in apparent affinity of about 100-fold.

The crystal structure of the IIA^{Glc}–GK(I474D) complex has been determined (Table 1). The I474D substitution causes no alterations of the secondary or tertiary structure

Figure 5

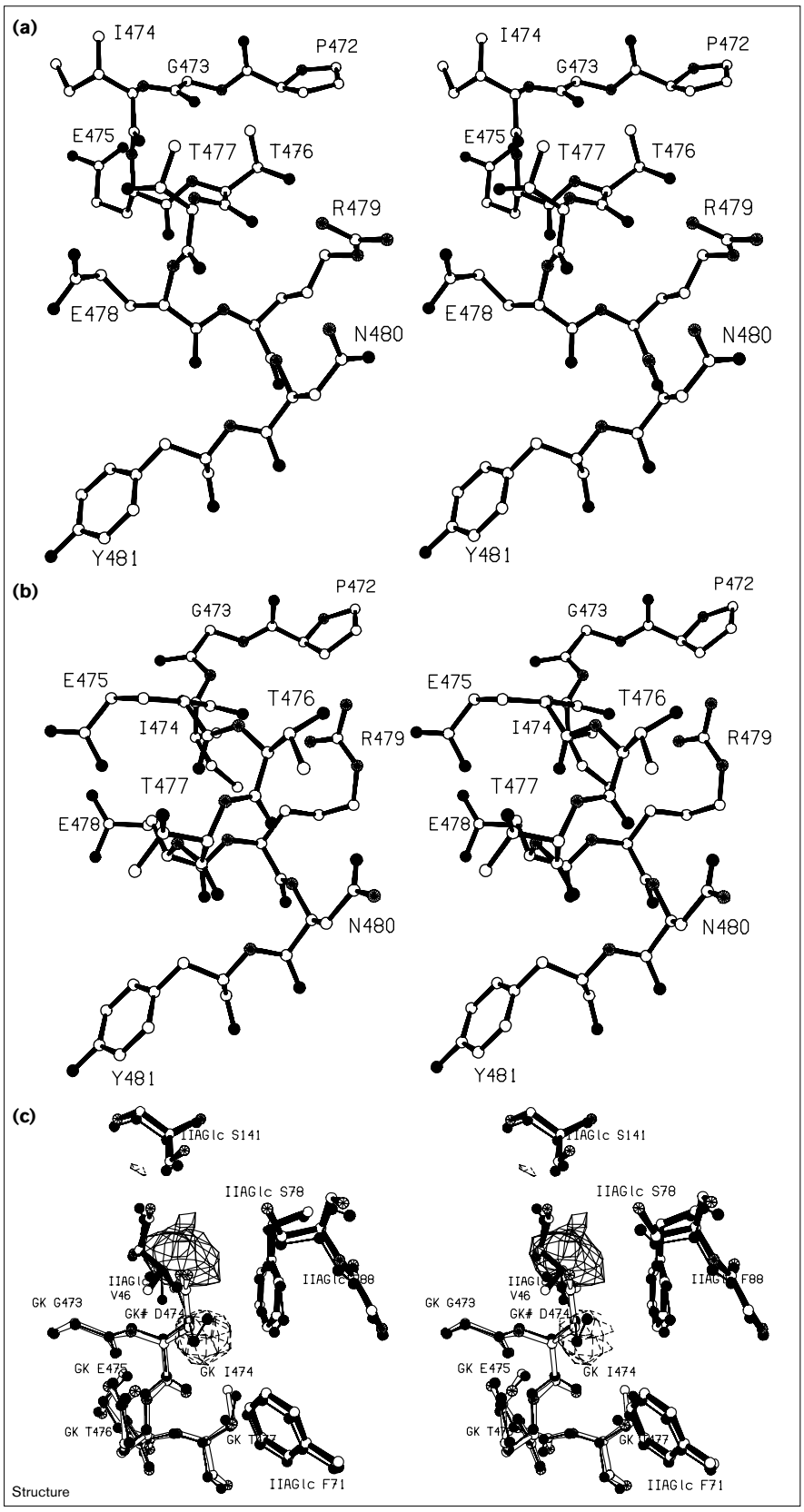

The IIA^{Glc}-binding site. **(a)** Stereoview of the conformation of the IIA^{Glc}-binding site in tetramer I (the IIA^{Glc}–GK complex). **(b)** Stereoview of the conformation of the IIA^{Glc}-binding site in tetramer II. **(c)** Stereoview of the I474D GK mutant in complex with IIA^{Glc} superimposed on the wild-type structure. GK residues are shown as open bonds with GK# denoting the mutant residue; IIA^{Glc} residues are shown in thick bonds. The wild-type structure is shown with filled atoms and thin filled bonds. $F_{obs(I474D)}$–$F_{obs(wild\ type)}$ difference electron density contoured at +6σ (solid lines) and −6σ (dashed lines) is superimposed on the final refined model.

Table 2

Kinetic constants for wild type and mutant glycerol kinases*.

Enzyme	V_{max} (U/mg)	K_{ATP} (μM)	K_{gol} (μM)	$K_{i,ATP}$ (μM)
Wild type	22 (18, 25)	16 (11, 21)	16 (10, 21)	30 (21, 43)
I474D	2.4 (2.3, 2.5)	2 (1.7, 3)	2 (1.3, 2.7)	17 (8, 25)
R479D	1.6 (1.4, 1.7)	2.5 (2.3, 2.4)	2 (1.4, 3.3)	8 (2, 13)

*The best-fit values of the parameters are given with confidence limits corresponding to one standard deviation given in parentheses.

and has no effect on the relative orientations of the GK and IIA^{Glc} molecules in the complex (Figure 5c). Similarly there are no apparent changes in substrate binding or conformation at the active site (data not shown). The aspartate residue is positioned such that the Cβ and Cγ atoms replace the hydrophobic contacts of the Cβ and Cγ2 of the isoleucine. The aspartate Oδ atoms face the solvent region and do not form any hydrogen bonds or salt bridges. It seems unlikely that the negatively charged Asp474 residue could assume the buried configuration of Ile474 seen in the tetramer II conformation (Figure 5b). Therefore, the conformational transition of the IIA^{Glc}-binding site appears to be an essential aspect of IIA^{Glc} regulation.

The orthophosphate-binding site

Residues 230–236 of subdomain IC are completely disordered in tetramer I, but are clearly visible and well ordered in each monomer of tetramer II where they form a binding site for orthophosphate and sulfate at the O–X interface. The average B factor for these loops is 33.2 $Å^2$ in wild-type GK and 39.9 $Å^2$ in the A65T mutant, almost the same as the overall average B factors in both cases. The average B factors for the bound phosphate and sulfate are 41.8 $Å^2$ and 53.3 $Å^2$, respectively. In order to confirm the binding of orthophosphate, a data set was taken from a crystal of wild-type GK in which the original mother liquor was replaced by a solution containing MOPS buffer instead of phosphate buffer. F_{obs}–F_{calc} omit electron-density maps calculated with this data set did not contain pyramid-shaped density features, as seen when phosphate was present. A similar experiment was not performed for the A65T mutant of GK. Nevertheless, the similar size and electronic configuration of orthophosphate and sulfate ions and the high concentration of sulfate in the mother liquor makes our interpretation reasonable.

The loops formed from residues 230–236 are Ω-shaped and bind the orthophosphate ion directly between them on the twofold axis (Figure 4). Four apparent water molecules are also bound beneath the orthophosphate and within the loops. The orthophosphate is bound by interaction with the backbone nitrogen atom of Gly234, the Nδ2 atom of Asn228, and Nη1 and Nη2 of Arg236, and contacts two bound water molecules. The loop structure is stabilized by three intramolecular hydrogen bonds (Asn228 Oδ1→Gly230 N, Thr235 Oγ1→Lys232 O and Arg236 Nε→Thr236 O) and two intermolecular hydrogen bonds (Asn228 Nδ2→Gly231 O and Asn228 O→Gly231 N), as well as by interaction with the bound water molecules and orthophosphate.

It was noted previously [25] that the sequence of residues 229–236 of the loop (Ile-Gly-Gly-Lys-Gly-Gly-Thr-Arg) is similar to a Walker-type glycine-rich nucleotide-binding sequence (P-loop sequence, Gly-x-x-Gly-x-Gly-Lys-Thr) [40], suggesting some functional role for these residues. P loops occur in a wide variety of nucleotide-binding proteins [41,42]. The high glycine content allows a mainchain conformation such that the backbone nitrogens of three or four residues point towards the inside of the loop and provide dipolar interactions with the phosphates of the bound nucleotide. The conserved lysine residue of the P loop stabilizes the phosphate's negative charge. Although the secondary structure context is different, the shape and phosphate interactions of the GK orthophosphate-binding loop are similar to the P loop, with Arg236 fulfilling the role of the conserved lysine residue. In nucleotide-binding proteins, however, the phosphate is bound by only one P loop, as opposed to being sandwiched between two as in GK.

This orthophosphate-binding site suggests a simple and appealing induced-fit mechanism for the FBP stabilization of the GK tetramer that was characterized by de Riel and Paulus [6–8]. FBP might form a ternary complex by binding its phosphates between the loops at the O–X interface, stabilizing the tetramer by direct interaction with both functional dimers. In fact, orthophosphate, sulfate and fructose-6-phosphate all exhibit inhibition of GK with K_i values of 89 mM, 110 mM and 125 mM, respectively (DWP, unpublished data). The inhibition is uncompetitive with respect to glycerol and noncompetitive with respect to ATP. The K_i for FBP, for comparison, is ~0.25 mM.

The circumstantial evidence for the orthophosphate-binding site also being the FBP regulatory binding site is strong. However, F_{obs}–F_{calc} omit electron-density maps calculated from data sets taken from crystals exchanged with mother liquor containing FBP or grown from mother liquor containing FBP showed no difference features that could be interpreted as bound FBP. A possible reason for this is that close crystal contacts near the apex of the orthophosphate-binding site in both the wild-type and A65T GK unit cells might sterically block FBP binding in these crystal forms. Therefore, a new crystal form of GK was investigated in order to observe bound FBP. The results of this study, which confirm that the orthophosphate-binding site is part of the FBP-binding site, will be presented elsewhere.

Discussion

GK is an intriguing candidate for investigating V-system regulation because, in addition to the homotropic nucleotide regulation, it has two heterotropic effectors that bind at widely separated sites yet appear to produce the same structural or dynamic changes at the active site. V system allosteric enzymes such as GK are rare, and a detailed regulatory mechanism has not yet been determined for any of the known examples. Two general types of mechanism can be envisioned for allosteric transitions. One is a global conformational change involving quaternary structure or domain motion; the other is a series of small rearrangements within one or both domains, such as reorientations of secondary structure, that transmit the effect of inhibitor binding from the distant allosteric sites to the active site of the enzyme. In order to understand the allosteric regulation of GK, structures of the active and inactive states of the enzyme must be elucidated and the mechanism by which inhibitor binding affects these structures must be established.

We have identified allosteric effector-binding sites in the IC (orthophosphate- and putative FBP-binding site) and IIC (IIA^{Glc}-binding site) subdomains of GK. These domains are both novel insertions in the ATPase core fold that are not found in other members of the superfamily [14]. Both effector-binding sites are ~30 Å from the active site, indicating that long range conformational changes are required to transmit the inhibitor-binding interaction to the active site.

Examination of the structure reveals that fairly direct connections do exist between both inhibitor-binding sites and the active site. The IC and IIC domains are both integrated into the ATPase core fold by contributing extra β strands to the N-terminal edges of the IA and IIA core β sheets, which form the binding sites for glycerol, the catalytic magnesium ion and the triphosphate moiety of ATP. Both inhibitor-binding sites are immediately adjacent to these extra β strands, suggesting a simple model in which the local conformational changes caused by inhibitor binding are transmitted by these connections to the active site.

PGDH from *E. coli* is also a tetramer of 222 symmetry with a striking overall resemblance to GK (Figure 2c); PGDH binds its allosteric effector, serine, at a subunit–subunit interface. A mechanism for the V system allosteric regulation of PGDH has been proposed in which binding of serine prevents a domain motion that is a necessary step in the catalytic cycle [33,43–45]. The serine-binding sites of PGDH, like the orthophosphate-binding sites of GK, are located at the tetramer-forming interface ~30 Å from the active site. Serine binding bridges the subunit–subunit interface between the regulatory domains and is thought to stabilize an open conformation of the enzyme, thus hindering a hinge-bending motion between the nucleotide- and substrate-binding domains that is required for catalysis. In PGDH the domain hinge is on the inside of the tetramer such that serine binding is proposed to restrain the active site in a open conformation, whereas in GK the hinge would be on the outside such that orthophosphate or FBP binding is proposed to restrain the active site in a closed conformation.

Regulatory mechanisms involving domain reorientations, as proposed for PGDH, are attractive models for V system allosteric enzymes, because it is easy to imagine how altering the dynamics of a domain motion required for catalysis would allow modulation of reaction rate without altering the binding constants of the substrates. Such a model can readily by applied to the regulation of GK by FBP. Like other members of its superfamily, GK is thought to undergo a large domain reorientation during catalysis, probably by means of a hinge-bending mechanism. Tetramer II appears to represent the FBP regulatory tetramer in the closed conformation, and it is apparent from the structure that any significant reorientation of the N- and C-terminal domains of GK would disrupt at least one of the O–X interfaces of tetramer II. FBP binding might thus achieve V-system regulation by creating an energetic barrier to domain reorientation.

However, FBP regulation depends on tetramerization whereas IIA^{Glc} regulation does not, arguing for a more complex mechanism. There is no obvious means by which IIA^{Glc} binding and its associated conformational change could alter the proposed domain motion. Nevertheless, the fact that both inhibitors result in essentially the same inactive monomeric form argues that the end result of inhibition is the same, regardless of the mechanistic details.

Biological implications

***Escherichia coli* glycerol kinase (GK) is a rare example of a velocity-modulated enzyme that catalyzes the rate-limiting step in glycerol utilization. The enzyme exists in a dimer↔tetramer equilibrium and is allosterically regulated by fructose-1,6-bisphosphate (FBP), the phosphotransferase system phosphocarrier protein IIA^{Glc} and adenosine nucleotides. FBP regulation depends upon tetramerization, whereas IIA^{Glc} and nucleotide regulation do not. Detailed mechanisms for velocity modulation of enzyme activity are not yet available for any such enzyme.**

Here we present a new tetrameric structure of GK (tetramer II) and compare it to the previously determined structure of a IIA^{Glc}–GK complex. A large change in the quaternary interactions within this new tetramer produce a more extensive dimer–dimer contact featuring efficient α-helical packing. Residues 230–236, which are disordered in the IIA^{Glc}–GK complex, become ordered in tetramer II and create an orthophosphate-binding site resembling a

nucleotide binding P loop. Orthophosphate regulates GK in the same manner as FPB, but the K_i is much higher. Thus the orthophosphate-binding site is proposed to form part of the FBP-binding site. The position of this site at the tetramer-forming interface is consistent with the role of tetramerization in FBP regulation. In addition, in tetramer II a 3_{10} helix involved in IIA^{Glc} binding is transformed into a short strand-like structure and an extra turn at the beginning of the last α helix. Amino acid substitutions in this region led to significantly altered kinetics and regulation, suggesting that this conformational transition is an essential aspect of IIA^{Glc} regulation. Possible mechanisms for the allosteric regulation of the activity are discussed in the light of the structural results.

Materials and methods

The site-directed mutants I474D and R479D were constructed, purified and characterized by previously described procedures [13,30]. Both mutations were verified by sequence determination of the entire mutant *glpK* gene. Wild-type and A65T GK were purified and wild-type GK was crystallized as described previously [46]. Protein concentrations were determined with the Bio-Rad protein assay and initial-velocity studies were performed as described previously [30].

Crystals of wild-type GK are in space group $P2_1$ with unit-cell dimensions $a = 92.1$, $b = 117.4$, $c = 108.4$ Å and $\beta = 93.1°$, the crystals contain a tetramer in the asymmetric unit. Crystals of the IIA^{Glc}–GK(I474D) mutant complex were prepared as described previously [26] and were isomorphous with the wild-type complex crystals. For crystallization purposes, A65T GK at 10 mg/ml was mixed with equal volumes of precipitant solution on silanized cover slips and suspended over wells on tissue-culture plates containing 0.5 ml of precipitant solution. Crystals were grown using the hanging-drop vapor diffusion method against 20–22% polyethylene glycol M_r 4000, 0.2 M lithium sulfate, and 0.1 M Tris (pH 8.5–8.8). The crystals are in space group $P2_1$ with unit-cell dimensions $a = 91.9$, $b = 119.0$, $c = 109.3$ Å and $\beta = 103.4°$; the crystals contain a tetramer in the asymmetric unit.

Diffraction data were collected with CuK^{α} radiation on a Rigaku RU-100 rotating-anode X-ray generator equipped with a graphite monochromator and operated at 40 kV, 150 mA. Data sets were collected with a San Diego Multiwire Detector Systems Mark III area detector [47] and were reduced using the supplied software [48].

Because the I474D IIA^{Glc}–GK complex crystallized isomorphously to that of wild-type GK, the structure was solved using F_{obs}(I474D)–F_{obs}(wild type) difference electron-density maps and the model refined. The final crystallographic R factor is 17.5% for all data between 21.0 Å and 2.37 Å (Table 1).

The $P2_1$ GK structures were solved by molecular replacement methods. Rotational correlation searches were performed using the program FRF SUM (W Kabsch, unpublished program), and translational searches were performed and rotation solutions refined with a brute-force R factor correlation search program (SJR, unpublished program). Atomic model refinement was performed with the TNT package [49], and electron-density maps were examined and model building performed with the programs FRODO [50], O [51] and Quanta (BIOSYM/MSI).

Solvent-accessible surface areas of intermolecular interfaces were calculated by the method of Lee and Richards [52], as implemented in the program EDPDB [53] using a probe radius of 1.4 Å and a step size of 0.2 Å. Gap volumes [54] between interfaces were calculated using the program SURFNET [55] with gap sphere radii between 1.4 and 4.0 Å. Plots of protein structures were prepared using the program MOLSCRIPT [56], ORTEP and RASTER3D [57].

Wild-type GK molecular replacement

Rotational correlation searches using data from 20–4 Å were performed using the GK coordinates from a single monomer of the refined structure of the IIA^{Glc}–GK complex as a search model (PDB accession code 1GLA). Two peaks at 16.3σ above the mean were observed (in both monoclinic crystals a molecular twofold axis is parallel to the crystallographic 2_1, so this result is expected). The next highest unique peak was 6.3σ above the mean. Translational correlation searches were carried out in an iterative manner using data from 20–4 Å. By adding the molecular transform of each correctly positioned monomer to the calculated structure factors, monomers were added successively until the model was complete.

The molecular replacement model, with an overall B factor of 25 $Å^2$, had an initial R factor of 51.6% for data from 20–4 Å, which dropped to 32.4% after five cycles of rigid-body refinement, with each monomer treated independently. Refinement was continued using the restrained least-squares method. Before the first round of model building the R factor was 24.1% for data from 20–2.6 Å.

($2F_{obs}$–F_{calc}) electron-density maps clearly suggested positions for both the glycerol and ADP substrates and there was clear electron density at the twofold tetramer (O–X) interfaces allowing residues 230–236, which were not visible in the electron-density map for the IIA^{Glc}–GK complex, to be built into the model. A large pyramid-shaped feature was visible in the electron density between the newly modeled loops at each interface and was modeled as orthophosphate because of the presence of phosphate buffer in the crystallization mother liquor. After several alternate rounds of refinement and model building, correlated B factors were used for further refinement. The final crystallographic R factor is 14.6% for all data between 20 Å and 2.62 Å (Table 1).

A65T GK mutant molecular replacement

Rotational correlation searches using data from 8–4 Å for observed and calculated structure factors were carried out using the GK coordinates from the refined wild-type tetramer as a search model with both the glycerol and ADP removed. Rotational and translational correlation searches were performed using data from 8–4 Å and proved to be straightforward, yielding peaks higher that 10σ above the mean. Refinement for A65T GK proceeded essentially as for wild-type GK. The electron density clearly suggested positions for the bound glycerol. Pyramid-shaped features, similar to those observed in the wild-type enzyme, were found between the loops formed by residues 230–236 at the twofold tetramer (O–X) interface. Similar features were also observed in the active site in approximately the position occupied by the β-phosphate of ADP and were modelled as sulfate. The final crystallographic R factor is 16.6% for all data between 20 Å and 2.37 Å (Table 1).

Accession numbers

The coordinates of wild-type GK and the A65T mutant have been submitted to the Brookhaven Protein Data Bank with accession codes 1GLF and 1BU6, respectively.

Acknowledgements

The authors are grateful for expert technical assistance by Wei Zhang Liu, Gayle Smith and Karen Kallio. This work was supported by National Institutes of Health (NIH) grants GM-49992 (DWP) and GM42618 (SJR).

References

1. Hayashi, S.-I. & Lin, E.C.C. (1967). Purification and properties of glycerol kinase from *Escherichia coli. J. Biol. Chem.* **242**, 1030-1035.
2. Zwaig, N., Kistler, W.S. & Lin, E.C. (1970). Glycerol kinase, the pacemaker for the dissimilation of glycerol in *Escherichia coli. J. Bacteriol.* **102**, 753-759.
3. Zwaig, N. & Lin, E.C.C. (1966). Feedback inhibition of glycerol kinase, a catabolic enzyme in *Escherichia coli. Science* **153**, 755-757.
4. Thorner, J.W. & Paulus, H. (1971). Composition and subunit structure of glycerol kinase from *Escherichia coli. J. Biol. Chem.* **246**, 3885-3894.
5. Thorner, J.W. & Paulus, H. (1973). Catalytic and allosteric properties of glycerol kinase from *Escherichia coli. J. Biol. Chem.* **248**, 3922-3932.

6. de Riel, J.K. & Paulus, H. (1978). Subunit dissociation in the allosteric regulation of glycerol kinase. 2. Physical evidence. *Biochemistry* **17**, 5141-5145.
7. de Riel, J.K. & Paulus, H. (1978). Subunit dissociation in the allosteric regulation of glycerol kinase from *Escherichia coli*. 3. Role in desensitization. *Biochemistry* **17**, 5146-5150.
8. de Riel, J.K. & Paulus, H. (1978). Subunit dissociation in the allosteric regulation of glycerol kinase from *Escherichia coli*. 1. Kinetic evidence. *Biochemistry* **17**, 5134-5140.
9. Postma, P.W., Epstein, W., Schuitema, A.R.J. & Nelson, S.O. (1984). Interaction between III^{glc} of the phosphoenolypyruvate:sugar phosphotransferase system and glycerol kinase of *Salmonella typhimurium*. *J. Bacteriol.* **158**, 351-353.
10. Novotny, M.J., Frederickson, W.L., Waygood, E.B. & Saier, M.H., Jr. (1985). Allosteric regulation of glycerol kinase by enzyme III^{glc} of the phosphotransferase system in *Escherichia coli* and *Salmonella typhimurium*. *J. Bacteriol.* **162**, 810-816.
11. Pettigrew, D.W., Yu, G. & Youguo, L. (1990). Nucleotide regulation of *Escherichia coli* glycerol kinase: initial-velocity and substrate binding sites. *Biochemistry* **29**, 8620-8627.
12. Voegele, R.T., Sweet, G.D. & Boos, W. (1993). Glycerol kinase of *Escherichia coli* is activated by interaction with the glycerol facilitator. *J. Bacteriol.* **175**, 1087-1094.
13. Pettigrew, D.W. (1998). Conserved active site aspartates and domain–domain interactions in regulatory properties of the sugar kinase superfamily. *Arch. Biochem. Biophys.* **349**, 236-245.
14. Hurley, J.H. (1996). The sugar kinase/heat shock protein 70/actin superfamily: implications of conserved structure for mechanism. *Annu. Rev. Biophys. Biomol. Struct.* **25**, 137-162.
15. Flaherty, K.M., McKay, D.B., Kabsch, W. & Holmes, K.C. (1991). Similarity of the three-dimensional structures of actin and ATPase fragment of a 70-kDa heat shock cognate protein. *Proc. Natl Acad. Sci. USA* **88**, 5041-5045.
16. Kabsch, W. & Holmes, K.C. (1995). The actin fold. *FASEB J.* **9**, 167-174.
17. Bork, P., Sander, C. & Valencia, A. (1992). An ATPase domain common to prokaryotic cell cycle proteins, sugar kinases, actin, and hsp70 heat shock proteins. *Proc. Natl Acad. Sci. USA* **89**, 7290-7294.
18. McDonald, R.C., Steitz, T.A. & Engelman, D.M. (1978). Yeast hexokinase in solution exhibits a large conformational change upon binding glucose or glucose 6-phosphate. *Biochemistry* **18**, 338-342.
19. Feldman, I. & Kramp, D.C. (1978). Fluorescence-quenching study of glucose binding by yeast hexokinase isoenzymes. *Biochemistry* **17**, 1541-1547.
20. Hoggett, J.G. & Kellett, G.L. (1976). Yeast hexokinase: substrate-induced association-dissociation reactions in the binding of glucose to hexokinase P-II. *Eur. J. Biochem.* **66**, 65-77.
21. Peters, B.A. & Neet, K.E. (1978). Yeast hexokinase PII. Conformational changes induced by substrates and substrate analogues. *J. Biol. Chem.* **253**, 6826-6831.
22. Miki, M. & Kouyama, T. (1994). Domain motion in actin observed by fluorescence resonance energy transfer. *Biochemistry* **33**, 10171-10177.
23. Drewes, G. & Faulstich, H. (1991). A reversible conformational transition in muscle actin is caused by nucleotide exchange and uncovers cysteine in position 10. *J. Biol. Chem.* **266**, 5508-5513.
24. Liberek, K., Skowyra, D., Zylicz, M., Johnson, C. & Georgopolous, C. (1991). The *Escherichia coli* DnaK chaperone, the 70-kDa heat shock protein eukaryotic equivalent, changes conformation upon ATP hydrolysis, thus triggering its dissociation from a bound target protein. *J. Biol. Chem.* **266**, 14491-14496.
25. Pettigrew, D.W., Ma, D.-P., Conrad, C.A. & Johnson, J.R. (1988). *Escherichia* glycerol kinase. Cloning and sequencing of the *glpK* gene and the primary structure of the enzyme. *J. Biol. Chem.* **263**, 135-139.
26. Hurley, J.H., *et al.*, & Remington, S.J. (1993). Structure of the regulatory complex of *Escherichia coli* III^{glc} with glycerol kinase. *Science* **259**, 673-677.
27. Feese, M., Pettigrew, D.W., Meadow, N.D., Roseman, S. & Remington, S.J. (1994). Cation promoted association (CPA) of a regulatory and target protein is controlled by protein phosphorylation. *Proc. Natl Acad. Sci. USA* **91**, 3544-3548.
28. Pettigrew, D.W., Feese, M., Neadow, N.D., Remington, S.J. & Roseman, S. (1994). Zn(II)-mediated protein interactions in *Escherichia coli* signal transduction: cation-promoted association of the phosphotransferase system regulatory protein III^{glc} with target protein glycerol kinase. In *Phosphate in Microorganisms: Cellular and Molecular Biology.* (Torriani-Gorini, A., Yagil, E. & Silver, S., eds), American Society for Microbiology, Washington, DC.
29. Pettigrew, D.W., Liu, W.Z., Holmes, C., Meadow, N.D. & Roseman, S. (1996). A single amino acid change in *Escherichia coli* glycerol kinase abolishes glucose control of glycerol utilization *in vivo*. *J. Bacteriol.* **178**, 2846-2852.
30. Pettigrew, D.W., Meadow, N.D., Roseman, S. & Remington, S.J. (1998). Cation-promoted association of *Escherichia coli* phosphocarrier protein IIA^{Glc} with regulatory target glycerol kinase: substitutions of a zinc(II) ligand and implications for inducer exclusion. *Biochemistry* **37**, 4875-4883.
31. Liu, W.Z., Faber, R., Feese, M., Remington, S.J. & Pettigrew, D.W. (1994). *Escherichia coli* glycerol kinase: role of a tetramer interface in regulation by fructose-1,6-bisphosphate and phosphotransferase system regulatory protein III^{glc}. *Biochemistry* **33**, 10120-10126.
32. Jones, S. & Thornton, J.M. (1996). Principles of protein–protein interactions. *Proc. Natl Acad. Sci. USA* **93**, 13-20.
33. Schuller, D.J., Grant, G.A. & Banaszak, L.J. (1995). The allosteric ligand site in the V_{max}-type cooperative enzyme phosphoglycerate dehydrogenase. *Nat. Struct. Biol.* **2**, 69-76.
34. Gerstein, M., Lesk, A.M. & Chothia, C. (1994). Structural mechanisms for domain movements in proteins. *Biochemistry* **33**, 6739-6747.
35. Walter, M.R., *et al.*, & Narula, S.K. (1995). Crystal structure of a complex between interferon-gamma and its soluble high-affinity receptor. *Nature* **376**, 230-235.
36. Jeffrey, P.D., *et al.*, & Pavletich, N.P. (1995). Mechanism of CDK activation revealed by the structure of a cyclin A–CDK2 complex. *Nature* **376**, 313-320.
37. Scheffzek, K., *et al.*, & Wittinghofer, A. (1997). The Ras–RasGAP complex: structural basis for ATPase activation and its loss in oncogenic mutants. *Science* **277**, 333-338.
38. Stein, P. & Chothia, C. (1991). Serpin tertiary structural transformation. *J. Mol. Biol.* **221**, 615-621.
39. Kelly, J.W. (1997). Amyloid fibril formation and protein misassembly: a structural quest for insights into amyloid and prion diseases. *Structure* **15**, 595-600.
40. Walker, J.E., Saraste, M., Runswick, M.J. & Gay, N.J. (1982). Distantly related sequences in the alpha- and beta-subunits of ATP synthase, myosin, kinases and other ATP-requiring enzymes and a common nucleotide binding fold. *EMBO J.* **1**, 945-951.
41. Saraste, M., Sibbald, P.R. & Wittinghofer, A. (1990). The P-loop – a common motif in ATP- and GTP-binding proteins. *Trends Biochem. Sci.* **19**, 430-434.
42. Bossemeyer, D. (1994). The glycine-rich sequence of protein kinases: a multifunctional element. *Trends Biochem. Sci.* **19**, 201-205.
43. Al-Rabiee, R., Lee, E.J. & Grant, G.A. (1996). The mechanism of velocity modulated allosteric regulation in D-3-phosphoglycerate dehydrogenase: cross-linking adjacent regulatory domains with engineered disulfides mimics effector binding. *J. Biol. Chem.* **271**, 13013-13017.
44. Al-Rabiee, R., Zhang, Y. & Grant, G.A. (1996). The mechanism of velocity modulated allosteric regulation in D-3-phosphoglycerate dehydrogenase: site-directed mutagenesis of effector binding site residues. *J. Biol. Chem.* **271**, 23235-23238.
45. Grant, G.A., Schuller, D.J. & Banaszak, L.J. (1996). A model for the regulation of D-3-phosphoglycerate dehydrogenase, a V_{max}-type allosteric enzyme. *Protein Sci.* **5**, 34-41.
46. Faber, H.R., Pettigrew, D.W. & Remington, S.J. (1989). Crystallization and preliminary X-ray studies of *Escherichia coli* glycerol kinase. *J. Mol. Biol.* **207**, 637-639.
47. Hamlin, R. (1985). Multiwire area X-ray diffractometers. *Methods Enzymol.* **114**, 416-452.
48. Howard, A.J., Nielsen, C. & Xuong, N.H. (1985). Software for a diffractometer with multiwire area detector. *Methods Enzymol.* **114**, 452-471.
49. Tronrud, D.E., Ten Eyck, L.F. & Matthews, B.W. (1987). An efficient general-purpose least-squares refinement program for macromolecular structures. *Acta Cryst. A* **43**, 489-503.
50. Jones, T.A. (1982). FRODO: a graphics fitting program for macromolecules. In *Computational Crystallography.* (Sayre, D., ed.), pp. 303-317, Oxford University Press, Oxford, UK.
51. Jones, T.A. (1978). A graphics model building and refinement system for macromolecules. *J. Appl. Cryst.* **11**, 268-272.
52. Lee, B. & Richards, F.M. (1971). The interpretation of protein structures: estimation of static accessibility. *J. Mol. Biol.* **55**, 379-400.
53. Zhang, X.J. & Matthews, B.W. (1995). EDPDB: a multi-functional tool for protein structure analysis. *J. Appl. Cryst.* **28**, 624-630.
54. Jones, S. & Thornton, J.M. (1995). Protein–protein interactions: a review of protein dimer structures. *Prog. Biophys. Mol. Biol.* **63**, 31-65.
55. Laskowski, R.A. (1995). SURFNET: a program for visualizing molecular surfaces, cavities and intermolecular interactions. *J. Mol. Graph.* **13**, 323-330.
56. Kraulis, P.J. (1991). MOLSCRIPT: a program to produce both detailed and schematic plots of protein structures. *J. Appl. Cryst.* **24**, 946-950.
57. Merrit, E. & Murphy, M. (1994). Raster3D version 2.0: a program for photorealistic molecular graphics. *Acta. Cryst. D* **50**, 869-873.